Supporting Information

Efficiency Boost in Perovskite Solar Cells via TiO_2 Nanodiscs Embedded in the $MoSe_2$ Electron Transport Layer Revealed by Optoelectronic Simulations

Javad Maleki[1∴], Maryam Shahrostami[1∴], Siming Huang[2], Mojtaba Abdi-Jalebi[2*]

[1] *Department of Electrical and Computer Engineering, Tarbiat Modares University (TMU), Tehran, Iran*

[2] *Institute for Materials Discovery, University College London, Malet Place, London, WC1E 7JE, United Kingdom*

∴ These authors contributed equally to this work.

* Corresponding author: m.jalebi@ucl.ac.uk

At the wavelength of 340 nm, the resonance was located in the middle of the TiO_2 nanodisc. Therefore, the electric field could not affect the light absorption in the materials around and above TiO_2, as shown in Fig. S1 (a). At the wavelength of 500 nm, as presented in Fig. S1 (b), the resonance still occurred in the nanodiscs, but it was located at the side edges of the nanodiscs, causing an increase in the electric field around the nanodiscs. Consequently, the electric field increment led to an increase in the light absorption around the nanodiscs at this wavelength. However, it should be noted that the intensity of the electric field at this wavelength was higher than other wavelengths. Also, at the wavelength of 740 nm (Fig. S1 (c)), the resonance of the electric field occurred in the space around and above the nanodiscs. If absorbent materials had been used instead of TiO_2, the intensity of the electric field would have increased, and as a result, the amount of light absorption would have been higher.

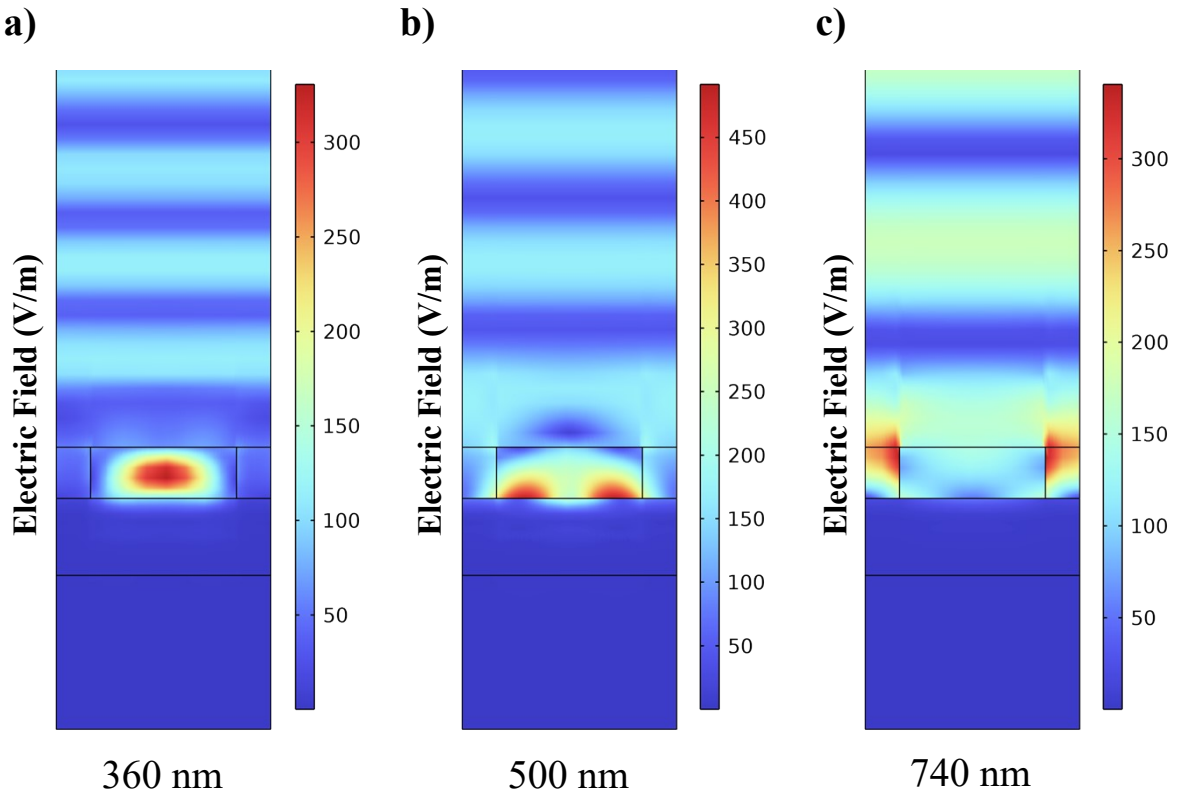

Figure S1. Electric field distribution for the TiO_2 nanodiscs metasurface reflector at different wavelength of **(a)** 360 nm, **(b)** 500 nm and **(c)** 740 nm.

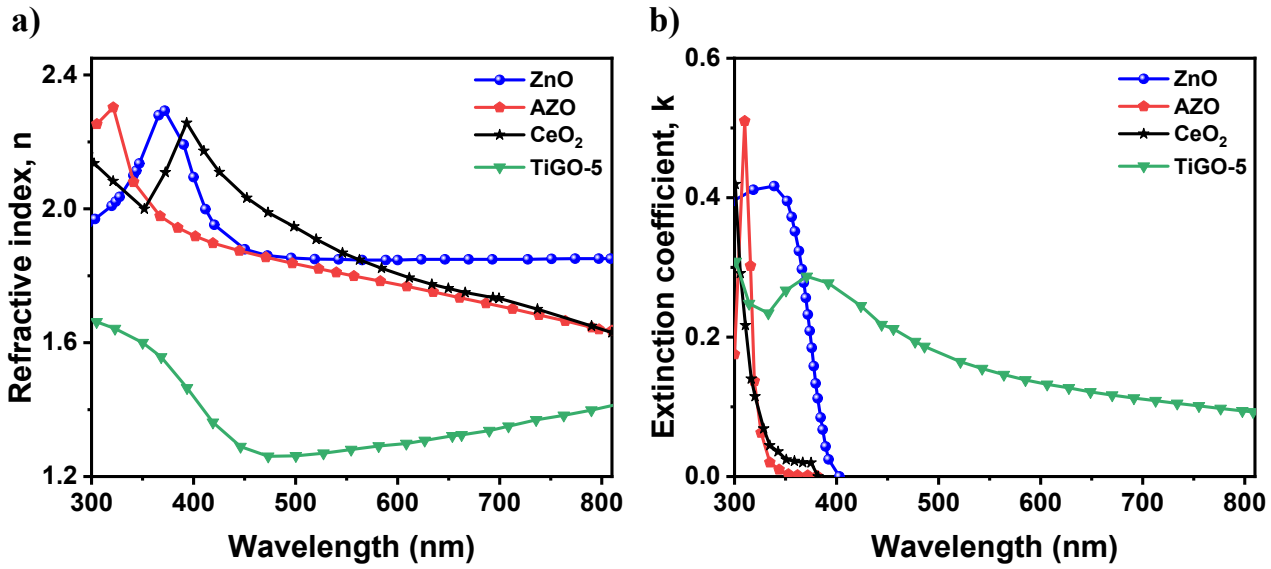

Figure S2. **(a)** refractive indices and **(b)** extinction coefficients for different materials around the TiO_2 nanodiscs. [1-4]

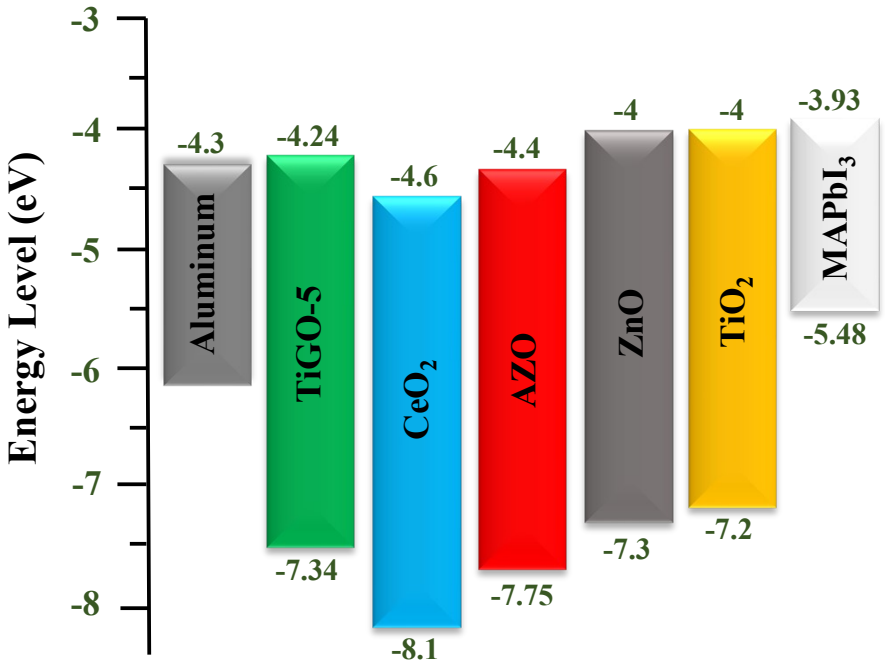

Figure S3. The band diagram of the Al, different ETL materials around the TiO_2 metasurface structure, and the perovskite (all the energy levels were taken from the references listed in Table 1).

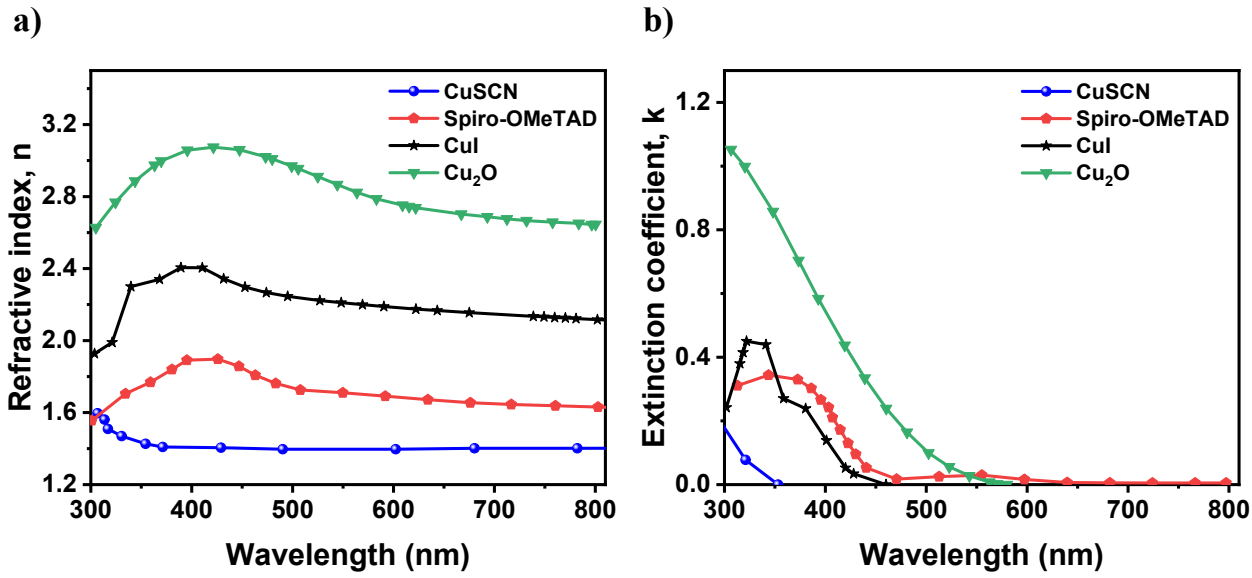

Figure S4. The **(a)** refractive indices, and **(b)** extinction coefficients for different HTL materials.[5-8]

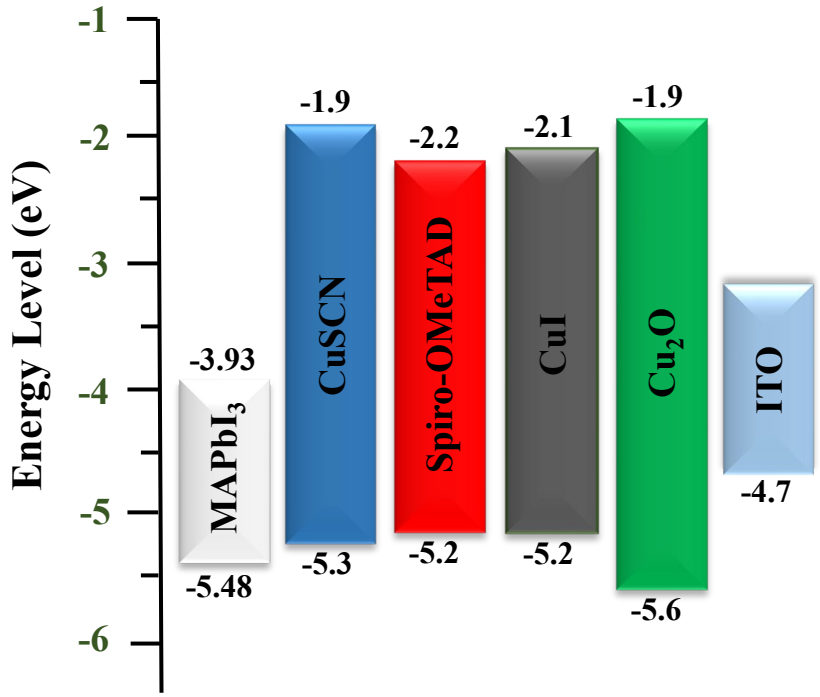

Figure S5. The band diagram of the perovskite, different HTL materials, and ITO (all the energy levels were taken from the references listed in Table 1).

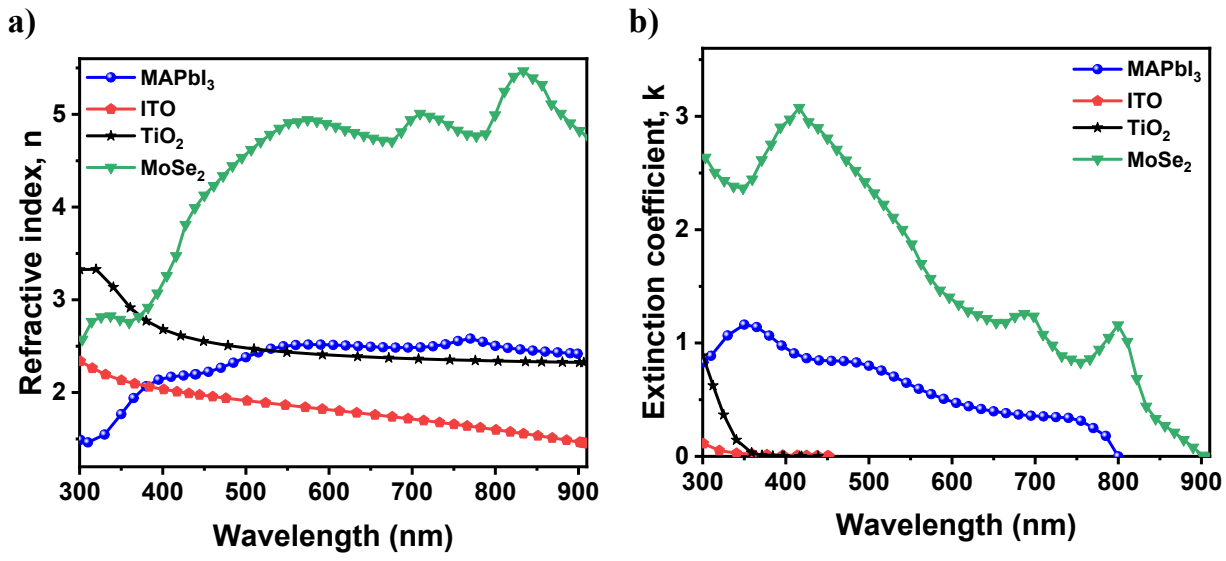

Figure S6. The **(a)** refractive indices, and **(b)** extinction coefficients of the other materials in the proposed solar cell. [6, 9]

References

(1) Zhai, C.-H.; Zhang, R.-J.; Chen, X.; Zheng, Y.-X.; Wang, S.-Y.; Liu, J.; Dai, N.; Chen, L.-Y. Effects of Al doping on the properties of ZnO thin films deposited by atomic layer deposition. *Nanoscale research letters* **2016**, *11*, 1-8.

(2) Nordseth, Ø.; Kumar, R.; Bergum, K.; Fara, L.; Dumitru, C.; Craciunescu, D.; Dragan, F.; Chilibon, I.; Monakhov, E.; Foss, S. E. Metal oxide thin-film heterojunctions for photovoltaic applications. *Materials* **2018**, *11* (12), 2593.

(3) Al-Bataineh, Q. M.; Telfah, M.; Ahmad, A. A.; Alsaad, A. M.; Qattan, I. A.; Baaziz, H.; Charifi, Z.; Telfah, A. Synthesis, crystallography, microstructure, crystal defects, optical and optoelectronic properties of ZnO: CeO2 mixed oxide thin films. In *Photonics*, 2020; MDPI: Vol. 7, p 112.

(4) Timoumi, A.; Alamri, S. N.; Alamri, H. The development of TiO2-graphene oxide nano composite thin films for solar cells. *Results in physics* **2018**, *11*, 46-51.

(5) Pattanasattayavong, P.; Ndjawa, G. O. N.; Zhao, K.; Chou, K. W.; Yaacobi-Gross, N.; O'Regan, B. C.; Amassian, A.; Anthopoulos, T. D. Electric field-induced hole transport in copper

(I) thiocyanate (CuSCN) thin-films processed from solution at room temperature. *Chemical Communications* **2013**, *49* (39), 4154-4156.

(6) Alnuaimi, A.; Almansouri, I.; Nayfeh, A. Effect of mobility and band structure of hole transport layer in planar heterojunction perovskite solar cells using 2D TCAD simulation. *Journal of computational electronics* **2016**, *15*, 1110-1118.

(7) Grundmann, M.; Schein, F. L.; Lorenz, M.; Böntgen, T.; Lenzner, J.; von Wenckstern, H. Cuprous iodide–ap-type transparent semiconductor: History and novel applications. *physica status solidi (a)* **2013**, *210* (9), 1671-1703.

(8) Bader, B.; Numan, N. H.; Khalid, F. G.; Fakhri, M. A.; Abdulwahab, A. ALL OPTICAL INVESTIGATIONS OF COPPER OXIDE FOR DETECTION DEVICES. *Journal of Ovonic Research* **2019**, *15* (1).

(9) Hsu, C.; Frisenda, R.; Schmidt, R.; Arora, A.; De Vasconcellos, S. M.; Bratschitsch, R.; van der Zant, H. S.; Castellanos-Gomez, A. Thickness-dependent refractive index of 1L, 2L, and 3L MoS2, MoSe2, WS2, and WSe2. *Advanced optical materials* **2019**, *7* (13), 1900239.